AIAA JOURNAL
Vol. 46, No. 3, March 2008

Switched Dynamic Systems for Reduced-Order Flow Modeling

Howard H. Hamilton*
U.S. Air Force Research Laboratory, Eglin Air Force Base, Florida 32542
and
Andrew J. Kurdila† and Anand K. Jammulamadaka‡
Virginia Polytechnic Institute and State University, Blacksburg, Virginia 24061

DOI: 10.2514/1.28896

We develop a family of reduced-order models for the modeling and control of a flow system operating under varying fluid and actuation parameters. The parametric subspaces of the reduced-order models are formed by considering the angle between the reduced-order subspaces that span the velocity fields. This grouping is combined with a discrete switching law to form a switched dynamic system composed of a set of reduced-order models. This methodology is applied to the modeling of a lid-driven cavity under varying translation velocities and phase differentials between the upper and lower walls. It is shown that the subspace angle metric successfully partitions the parametric space and provides insight on the dominant parameters that characterize the flowfields. An open-loop simulation of the resulting switched dynamic system demonstrates its ability to capture the evolution of the flow and input parameters as it occurs in the full-order model.

Nomenclature

$c_i(t)$	=	time-varying control inputs
E	=	edges on the undirected graph
f	=	excitation frequency, Hz
G_r	=	undirected graph, represents a partition of the parametric set
$\boldsymbol{g}$	=	generalized boundary-control function
h_0	=	fixed boundary-condition function
K	=	number of switching intervals
M	=	number of controls
N	=	number of reduced states
$\mathbb{N}$	=	index time set, $\{1, \ldots, N_t\}$
P, Q	=	number of parametric values
p	=	pressure
R	=	number of subsets of the parametric set
Re	=	Reynolds number
St	=	Strouhal number
t	=	time
U_0	=	mean or centerline velocity
u	=	horizontal velocity component
$\boldsymbol{V}$	=	fluid velocity in the inertial frame
v	=	vertical velocity component
$\boldsymbol{X}$	=	vector of state variables
$\boldsymbol{x}$	=	coordinate vector
x	=	horizontal coordinate
x_i	=	generalized coordinate, $i = 1, 2$
y	=	vertical coordinate
α_i	=	finite-dimensional states
$\boldsymbol{\beta}$	=	vector of control variables
β_0	=	control boundary-condition function
Γ	=	domain
Λ	=	flow/actuation parametric set
λ	=	input or actuation parameter
∂	=	boundary
Θ	=	$1/(Re \cdot St)$
θ_a	=	angle between subspaces
θ_{th}	=	upper bound of the subspace angle
ν	=	kinematic viscosity
$\boldsymbol{\xi}$	=	generalized function
τ	=	switching interval
ϕ	=	excitation-phase lag, deg
$\boldsymbol{\phi}$	=	generalized vector field
$\phi_c(\boldsymbol{x})$	=	spatial control influence function
Ω	=	domain

Subscripts

C	=	boundary-control conditions
c	=	control
D	=	Dirichlet boundary conditions on $\boldsymbol{V}$
PS	=	pseudo-stress-free boundary conditions
s	=	states
0	=	nominal or time-invariant conditions

I. Introduction

FLOW control has become an area of increasing interest within the fluid mechanics and control systems communities. Much progress has been made in the development of sensors [1], actuators [2], and control algorithms [3] to attenuate or exploit flow phenomena in engineering problems. These advances can be applied to a variety of problems related to combustion, biofluidics, acoustics, and aerodynamics. One specific challenge in flow control research involves the development of suitable models for control that are derived from the Navier–Stokes equations. These models are difficult to develop because of the inherent nonlinearity and infinite-dimensionality of the governing equations.

Reduced-order models are necessary to create feasible controllers for flow problems. In the past 30 years, some of the most popular techniques for the development of low-dimensional, nonlinear evolution equations representing the Navier–Stokes equations have been based on the method of proper orthogonal decomposition (POD). POD is an order-reduction technique that extracts the most

Presented as Paper 6191 at the AIAA Guidance, Navigation, and Control Conference, Keystone, CO, 21–24 August 2006; received 17 November 2006; revision received 28 November 2006; accepted for publication 18 July 2007.

*National Research Council Research Associate, Guidance, Navigation, and Control Branch, Munitions Directorate. Member AIAA.
†W. Martin Johnson Professor, Department of Mechanical Engineering. Associate Fellow AIAA.
‡Postdoctoral Associate, Department of Mechanical Engineering.

energetic modes from numerical or experimental flow simulations. POD models have been shown to effectively capture the essential physics of the flow, but several researchers have shown that a strict reduction of the flow physics to their most energetic modes is not sufficient for closed-loop control [4]. Moreover, the resulting reduced-order model is only applicable for a single flow regime. The essential difficulty is that the POD generates a single low-dimensional subspace in which the dynamics evolve over time.

A recent study by Fitzpatrick et al. [5] developed a modeling and control strategy to address flow control problems over varying regimes. It created a series of reduced-order models based on the phase difference between velocity fluctuations on both sides of a rectangular cavity, and it synthesized a linear parameter-varying (LPV) controller to reduce the disturbances within the cavity. Each reduced-order model represented the subspace of a full-scale flow, and so the control was scheduled across subspaces of the full state.

Other researchers have addressed the problem of modeling for varying conditions from a diversity of perspectives. Ravindran [6] used an adaptive scheme that updated the data ensemble from which a reduced-order basis is derived. This algorithm was demonstrated on a backward-facing step with blowing actuation and was effective in capturing the energy of the actuated flow system. Fahl [7] used trust-region methods to update the reduced-order model through an optimization-based approach. Jørgensen et al. [8] developed a sequential POD algorithm by which the data are organized into blocks and POD is performed sequentially on each block in the subspace orthogonal to the preceding blocks. These blocks correspond to data taken for different parametric values.

The approach described in this publication draws from concepts of hybrid dynamic systems. These systems are characterized by interactions between continuous dynamics and discrete automata [9]. Switched dynamic systems are a subset of hybrid dynamic systems in which the behavior is described as a finite collection of dynamic models with a set of rules that govern switching between the models. Examples of switched dynamic systems can be found in the book by Liberzon [10] and the references found therein. In our work, we develop a family of reduced-order models for fluid flows that operate under time-varying input and actuation parameters. We propose an approach in which the parameter space is partitioned into smaller regions using concepts from image cross-correlation and graph theory, based on a metric of the subspace angle between different flowfields. A reduced-order model is then associated with each region and a hypothesis-testing algorithm is developed to implement switching between regions. It will be shown that the collection of reduced-order dynamics over the operating domain can be described as a switched dynamic system. The evolution of the reduced-order representation of the dynamics develops as the trajectory "wanders" along several low-dimensional subspaces.

The organization of the paper is as follows. Section II derives the procedures that create the switched dynamic system, which is composed of the reduced-order system, the regions in which they reside, and the switching laws between regions. This approach is applied to the modeling of a two-sided lid-driven cavity in Sec. III. Section IV concludes with a summary of the results and their implications for future research.

II. Dynamic System Framework

In this paper, we define a framework for a dynamic system that describes the fluid flow in a two-dimensional domain Ω, illustrated in Fig. 1. The domain is enclosed by piecewise smooth boundaries $\partial\Omega$. The velocity and pressure fields within the domain are governed by the incompressible Navier–Stokes equations and the conservation of continuity,

$$\left.\begin{array}{c} \frac{\partial \boldsymbol{V}}{\partial t} + \frac{1}{St}\sum_{j=1}^{2} V_j \frac{\partial \boldsymbol{V}}{\partial x_j} + \nabla p = \Theta \Delta \boldsymbol{V} \\ \nabla \cdot \boldsymbol{V} = 0 \end{array}\right\} \quad \forall\ (\boldsymbol{x}, t) \in \Omega \times [0, T] \quad (1)$$

subject to the initial and boundary conditions:

$$\boldsymbol{V}(0) = \boldsymbol{V}_0 \qquad \forall \boldsymbol{x} \in \Omega \qquad \boldsymbol{V} = \boldsymbol{g} \quad \forall\ (\boldsymbol{x}, t) \in \partial\Omega \times [0, T] \quad (2)$$

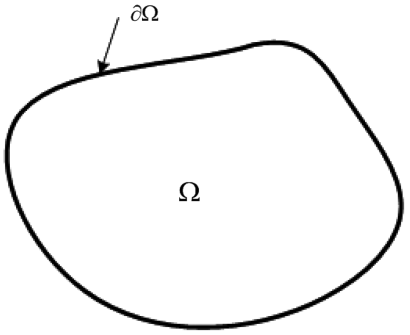

Fig. 1 Schematic of a two-dimensional flow domain.

We assume that there exists a set of velocity fields for an unordered list $\{\lambda\}$ of flow and/or actuation parameters that are of interest to the researcher. The collection forms a parametric set $\Lambda = (\lambda_p, \lambda_q)$, where λ_p and λ_q define parameters of interest that contain P and Q elements, respectively.

A. Reduced-Order Model for Flow Simulation

The strong form requires that all the derivations are understood in the classical sense. It is well known that this degree of regularity can be difficult to guarantee a priori; therefore, we seek a weak formulation. Moreover, model-based methodologies that generate a reduced-order flow model (in contrast to nonparametric identification techniques) typically use the weak form of these equations as a starting point. The weak form of the governing equations can be obtained in the usual way by taking the inner product of the strong form of the equations with a sufficiently smooth function $\boldsymbol{\xi}$ and integrating (by parts) over the domain Ω. It has become standard to represent the resulting weak form of the governing equations in terms of a bilinear form $a(\cdot,\cdot)$, trilinear form $b(\cdot,\cdot,\cdot)$, and a bilinear form $c(\cdot,\cdot)$, which are defined to be

$$a(\boldsymbol{U}, \boldsymbol{V}) = \Theta \int_{\Omega} (\boldsymbol{\nabla U}) : (\boldsymbol{\nabla V})\, \mathrm{d}\Omega \quad (3)$$

$$\frac{1}{St} b(\boldsymbol{U}, \boldsymbol{V}, \boldsymbol{W}) = \sum_{i,j}^{2} \int_{\Omega} U_j \frac{\partial V_i}{\partial x_j} W_i \, \mathrm{d}\Omega \quad (4)$$

and

$$c(\boldsymbol{V}, p) = \int_{\Omega} (\boldsymbol{\nabla} \cdot \boldsymbol{V}) p \, \mathrm{d}\Omega \quad (5)$$

respectively. It is easy to show that the aforementioned simple integration by parts yields the equations

$$\left\langle \frac{\partial \boldsymbol{V}(t)}{\partial t}, \boldsymbol{\xi} \right\rangle + a(\boldsymbol{V}(t), \boldsymbol{\xi}) + b(\boldsymbol{V}(t), \boldsymbol{V}(t), \boldsymbol{\xi}) - c(\boldsymbol{\xi}, p(t)) + \underbrace{\int_{\partial\Omega} p(t) \boldsymbol{\xi} \cdot \boldsymbol{n} \, \mathrm{d}S}_{I_1} - \underbrace{\int_{\partial\Omega} \boldsymbol{\xi} \cdot \frac{\partial \boldsymbol{V}(t)}{\partial n} \, \mathrm{d}S}_{I_1} = 0 \quad (6)$$

and

$$c(\boldsymbol{V}(t), q) = 0 \quad (7)$$

The terms I_1 and I_2 are defined in detail once the boundary conditions are specified. We want to keep the derivation as general as possible. Thus, we represent the boundary of the domain as the union

$$\partial\Omega = \partial\Omega_D + \partial\Omega_c + \partial\Omega_{\mathrm{PS}} \quad (8)$$

We briefly review the rigorous formulation of this flow control problem and the well-posedness of the formulation. This transformation requires a bit of functional analytic terminology. We denote the space of square integrable functions over the domain

Ω via

$$L^2(\Omega) = \left\{ f\colon \Omega \longrightarrow \mathbb{R}\colon \|f\|^2_{L^2(\Omega)} \equiv \int_\Omega |f(x)|^2 \, \mathrm{d}\Omega \right\} \tag{9}$$

Because the pressure field is determined only up to a normalizing constant, we will also require the subspace $L^2_0(\Omega)$ of zero-mean square integrable functions:

$$L^2_0(\Omega) = \left\{ p \in L^2(\Omega)\colon \int_\Omega p \, \mathrm{d}\Omega = 0 \right\} \tag{10}$$

The space $L^2(\Omega)$ is a collection of real-valued functions. Often, we will require functions that take values in some space X. The function space $L^p(0, T; X)$ is defined to be the collection of (Bochner integrable) functions $f\colon (0, T) \to X$, such that the norm

$$\|f\|^p_{L^p(0,T;X)} = \int_0^T \|f(t)\|^p_X \, \mathrm{d}t \tag{11}$$

is finite.

The Sobolev space $H^1(\Omega)$ denotes the collection of all the functions in $L^2(\Omega)$ for which the first weak derivative is also in $L^2(\Omega)$. It is well known that $H^1(\Omega)$ is a complete normed vector space when endowed with the usual norm:

$$\|f\|^2_{H^1(\Omega)} = \|f\|^2_{L^2(\Omega)} + \|\nabla f\|^2_{L^2(\Omega)} \tag{12}$$

We define

$$\mathbb{H}^1(\Omega) = [H^1(\Omega)]^2 \tag{13}$$

and

$$\mathbb{H}^1_0(\Omega) = \{ \boldsymbol{V} \in \mathbb{H}^1(\Omega)\colon \boldsymbol{V}|_{\partial\Omega - \partial\Omega_{\mathrm{PS}}} = 0 \} \tag{14}$$

The weak form of the governing equations seeks to find the pair $(\boldsymbol{V}, p) \in L^2(0, T; \mathbb{H}^1(\Omega)) \times L^2(0, T; L^2_0(\Omega))$, such that

$$\left\langle \frac{\partial \boldsymbol{V}(t)}{\partial t}, \boldsymbol{\xi} \right\rangle + a(\boldsymbol{V}(t), \boldsymbol{\xi}) + b(\boldsymbol{V}(t), \boldsymbol{V}(t), \boldsymbol{\xi}) - c(\boldsymbol{\xi}, p(t)) = 0 \tag{15}$$

and

$$c(\boldsymbol{V}(t), q) = 0 \tag{16}$$

for all pairs $(\boldsymbol{\xi}, q) \in \mathbb{H}^1_0(\Omega) \times L^2_0(\Omega)$, where $\boldsymbol{V}|_{\partial\Omega_D} = \boldsymbol{g} \in L^2(0, T; H^{\frac{1}{2}}(\partial\Omega_D))$ and $\boldsymbol{V}(0) = \boldsymbol{V}_0 \in L^2(\Omega)$.

The fundamental assumption underlying the reduced-order models derived in this paper is that the velocity field $\boldsymbol{V}$ can be approximated as

$$\boldsymbol{V}(t, \boldsymbol{x}) = \boldsymbol{\phi}_0(\boldsymbol{x}) + \underbrace{\sum_{i=1}^{M} c_i(t) \boldsymbol{\phi}_{c,i}(\boldsymbol{x})}_{V_c} + \underbrace{\sum_{i=1}^{N} \alpha_i(t) \boldsymbol{\phi}_{s,i}(\boldsymbol{x})}_{V_s} \tag{17}$$

The following assumptions hold on the vector fields appearing in the preceding expansion:

Assumption 1: $\boldsymbol{\phi}_0$, $\{\boldsymbol{\phi}_{c,i}\}_{i=1}^M$, and $\{\boldsymbol{\phi}_{s,j}\}_{j=1}^N$ are divergence-free.

$$\nabla \cdot \boldsymbol{\phi}_0 = 0 \tag{18}$$

$$\nabla \cdot \boldsymbol{\phi}_{c,i} = 0 \qquad i = 1, \ldots, M \tag{19}$$

$$\nabla \cdot \boldsymbol{\phi}_{s,j} = 0 \qquad j = 1, \ldots, N \tag{20}$$

Assumption 2: $\{\boldsymbol{\phi}_{s,i}\}_{i=1}^N$ satisfy zero boundary conditions on $\partial\Omega_c \cup \partial\Omega_D$.

Assumption 3: $\{\boldsymbol{\phi}_{c,i}\}_{j=1}^M$ satisfy zero boundary conditions on $\partial\Omega_D$.

Assumption 4: $\boldsymbol{\phi}_0$ satisfies the steady inhomogeneous boundary conditions on $\partial\Omega_D$:

$$\boldsymbol{\phi}_0|_{\partial\Omega_D} = f \tag{21}$$

$$\boldsymbol{\phi}_0|_{\partial\Omega_c} = 0 \tag{22}$$

Assumption 5: $\boldsymbol{V}_c$ satisfies the control boundary conditions

$$\boldsymbol{V}_c|_{\partial\Omega_c} = g \tag{23}$$

Suppose we have at our disposal the results of either a single simulation or a single experimental test that provides a time-indexed collection

$$\{(\boldsymbol{V}_k, p_k)\}_{k\in\mathbb{N}} \equiv \{(\boldsymbol{V}(t_k), p(t_k))\}_{k\in\mathbb{N}} \tag{24}$$

associated with a set of operating conditions (e.g., Reynolds number, Strouhal number, control and boundary conditions) that are fixed for this sequence. The problem of creating a reduced-order model now reduces to defining the functions $\boldsymbol{\phi}_0$, $\{\boldsymbol{\phi}_{c,i}\}_{i=1}^M$, and $\{\boldsymbol{\phi}_{c,j}\}_{j=1}^N$ from the discrete transient history in Eq. (24). If there is a single control input, the control influence is realized by the boundary condition

$$\boldsymbol{V}|_{\partial\Omega_c} = c(t)\boldsymbol{\phi}_c(\boldsymbol{x}) \quad \forall\ (t, \boldsymbol{x}) \in [0, T] \times \partial\Omega_c \tag{25}$$

For each subspace calculated and embodied in the choice of bases $\phi_0, \{\phi_{c,i}\}_{i=1,\ldots,M}$ and $\{\phi_{s,i}\}_{i=1,\ldots,N}$, a subspace-specific set of nonlinear ordinary differential equations is obtained when the ansatz for the velocity $\boldsymbol{V}(t)$ is substituted in the weak form of the governing equations:

$$\begin{aligned}\dot{\alpha}_i(t) = a_i &+ \sum_{k=1,\ldots,N} b_{ik}\alpha_k(t) + \sum_{\substack{k=1,\ldots,N\\ l=1,\ldots,N}} c_{ikl}\alpha_k(t)\alpha_l(t) \\ &+ \sum_{k=1,\ldots,N} d_{ik}\dot{c}_k(t) + \sum_{k=1,\ldots,N}\left(e_{ik} + \sum_{j=1,\ldots,N} f_{ijk}\alpha_j(t)\right)c_k(t) \\ &+ \sum_{\substack{k=1,\ldots,N\\ l=1,\ldots,N}} g_{ikl}c_k(t)c_l(t)\end{aligned}$$

The reader is referred to the derivations by Rediniotis et al. [11] and Ravindran [6] for a detailed discussion of this transformation. These nonlinear ordinary differential equations can be cast in a "control canonical" form with the introduction of the extended set of state variables $\boldsymbol{X}(t) = \{\boldsymbol{\alpha}(t)\boldsymbol{c}(t)\}^T$ and a new set of controls $\boldsymbol{\beta}(t) = \dot{\boldsymbol{c}}(t)$. These equations can be written as

$$\dot{X}(t) = \boldsymbol{F}(\boldsymbol{X}(t), t) + \boldsymbol{B}(\boldsymbol{X}(t))\boldsymbol{\beta}(t) \tag{26}$$

B. Switched Dynamic System

Repeated for a collection of elements in the parametric set, we generate several sets of basis functions associated with different operating conditions, which in turn gives rise to several sets of low-dimensional governing equations. These governing equations are indexed by the subspace over which the dynamics were restricted. These subspaces correspond to subsets of the complete parametric set. We use the notation found in Seidman's [12] work on switched systems to write a formal definition of the switched dynamic system:

$$\dot{\boldsymbol{X}}(t) = \boldsymbol{F}_{j(t)}(\boldsymbol{X}(t)) + \boldsymbol{B}_{j(t)}(\boldsymbol{X}(t))\boldsymbol{\beta}(t) \tag{27}$$

with $\boldsymbol{F}$ and $\boldsymbol{B}$ valid in the regions $\mathcal{R}_j$, $j \in \mathcal{J} = \{1, \ldots, R\}$. We say that $\beta(t)$ is measurable, $\boldsymbol{X}(t)$ is continuous, and $j(t)$ is subject to the following switching rules:

Definition 1: If $\boldsymbol{X} \in \partial\mathcal{R}_k$ for some $t \in [0, T]$ and $k \in \mathcal{J}$, then $\boldsymbol{X} \in \mathcal{S}_{k(t-),k(t+)}$.

In the preceding description, the region $\mathcal{R}_j$ contains the reduced-order states associated with a particular subset of the parametric set. The switching sets $\mathcal{S}_{j,k}$ govern the transition between regions $\mathcal{R}_j$ and

$\mathcal{R}_k$. The following two sections describe procedures to formulate $\mathcal{R}_j$ and $\mathcal{S}_{j,k}$.

C. Clustering of Subspaces and Parameter Sets

The previous section presented a general method to create a reduced-order model for a system operating in a particular flow regime. It is assumed that the experimental or computational flowfield used to develop the model is characterized by a set of intrinsic parameters such as the Reynolds number, inflow velocity magnitude, inflow velocity amplitude, inlet pressure, etc. Thus, each operating condition under study is associated with a specific set of parameter values characterizing the flow. The transient response of the flow for particular values of the intrinsic parameters, in turn, determine the approximating subspaces used to generate the reduced-order models. For notational simplicity, we consider only two such parameters in the remainder of this paper: p and q. The extension to an arbitrary, but fixed, number of parameters is straightforward. The set of values that the parameters p and q may take in developing the reduced-order model is denoted as $\Lambda = \{p_i, q_j\}_{i=1,\ldots,M, j=i,\ldots,N}$. If the number of values considered for each parameter is substantial, the curse of dimensionality can yield a prohibitive number of combinations (p_i, q_j) for $i = 1, \ldots, M$ and $j = 1, \ldots, N$. Recall that each such pair (p_i, q_j) generates an approximating subspace and, consequently, an associated reduced-order model.

It is therefore important to determine which subspaces, and consequently which reduced-order models, are nearly identical or redundant. There is no reason a priori to know that any particular subset of parameters will generate reduced-order models that are similar, or widely varying, in the transient response they generate.

We use a simple metric to measure the similarity between the approximating subspaces associated with particular values of the parameters. Suppose that $\boldsymbol{V}_0$ and $\boldsymbol{V}_1$ are two discrete vector fields defined over the same grid. Each field can be said to be approximated by a reduced-order basis that spans a subspace. The angle between these subspaces is defined to be

$$\theta_a = \cos^{-1}\left(\frac{\boldsymbol{V}_0 \cdot \boldsymbol{V}_1}{\|\boldsymbol{V}_0\|\|\boldsymbol{V}_1\|}\right) \tag{28}$$

The approximating subspaces used in the development of the reduced-order models of the last section are not, in general, one-dimensional. But this definition suffices to illustrate the type of measures generally used to calculate the level of "redundancy" in collections of subspaces. It is worth noting that the calculation of the angle between the preceding subspace is nothing more than a calculation of the correlation between two particular discrete vector fields. The definition of the calculation of the angle between subspaces in the case in which the subspaces have different dimensions (not necessarily equal to one!) is given in many places in the literature, such as that by Golub and van Loan [13]. Suffice it to say that the calculation of the angle between subspaces in this more general case can be determined via a direct application of the singular value decomposition.

A simple calculation illustrates that the number of reduced-order models, or approximating subspaces, that are generated as more values of the intrinsic parameters are considered grows in a combinatorial fashion. If there are $\mathcal{N} = M \cdot N$ distinct combinations of values of the parameters, then there are $\mathcal{N} \cdot (\mathcal{N} - 1)/2$ comparisons between approximating subspaces that must be carried out. In the most optimistic case, perhaps all the approximating subspaces are identical. Thus, only one reduced-order model need be retained in the final analysis. In the worst case, all of the combinations of values of the parameters generate distinct and nonnegligible approximating subspaces. In this case, the number of reduced-order models that should be retained in the final analysis would be $\mathcal{N} \cdot (\mathcal{N} - 1)/2$.

Fortunately, in some cases, the collection of all approximating subspaces do contain subcollections that span "nearly the same" subspace. This fact will be made clear in an example considered later in this paper. One approach that we use to reduce the number of redundant approximating subspaces, and therefore the number of reduced-order models, uses elements of graph theory (cf. Dodel et al. [14]). The elements of θ_a^{ij} constitute the weights of the edges on an undirected graph $G_r = (\Lambda, E)$ $(r = 1, \ldots, R)$. A threshold value $a_{\text{th}} \in (0, 1)$ is defined to be the maximum value used to define a subgraph $G_r(a_{\text{th}}) = (\Lambda^r(a_{\text{th}}), E^r(a_{\text{th}}))$, where

$$E^r(a_{\text{th}}) = \{(i, j) | c_{ij} \geq \theta_{\text{th}}\} \subseteq E \tag{29}$$

and

$$\Lambda^r(a_{\text{th}}) = \{i | (i, j) \in E^r(a_{\text{th}}) \vee (j, i) \in E^r(a_{\text{th}})\} \tag{30}$$

where $1 \leq i \leq P$ and $1 \leq j \leq Q$. Each G_r represents a partition of the parametric space into subspaces in which the velocity fields exhibit high cross-correlations. The vertices are the most important elements of the graph because they are used to define the parametric subspaces:

$$\mathcal{R}_r = \{\Lambda | \Lambda \in \Lambda^r(a_{\text{th}})\} \tag{31}$$

D. Discrete Switching Law

It is now left to develop a hypothesis-testing algorithm that governs switching between dynamic systems. Over a time interval $t \in [0, T]$, we assume that there exist K switching intervals $\tau_j \in [t_j t'_j]$, where $t'_j = t_{j+1}$ and $t'_K = T$ $(j = 1, \ldots, K)$. Furthermore, exogenous disturbances and control inputs across switching instants are assumed to be continuous. The reduced-order model is simulated for the switching interval, and at each switching instant t'_j, the velocity field is compared with a library of steady-state flow solutions over $\mathcal{R}_r$ (resulting in a 2-norm error measure), and the subspace that corresponds to the region of the smallest error measure is selected. Continuity of the velocity vector across switching intervals is maintained by adding an extra term to the velocity and using a cubic spline technique to drive the term to zero during the switching instant. A pseudocode of the implementation of the switched system is as follows:

```
begin
  → V_0, λ_0
  → τ_j, j = 1, ..., r
  → β(t)
  k ← λ_0 ∈ R_k
  j ← 1
  repeat
    α_0 ← ⟨V, φ^k⟩
    α̇ ← F_k(α(t)) + B_k(α(t))β(t), t ∈ τ_j
    V_POD ← V_m + Σ α(t)φ^k(x)
    ε(g) ← ‖V_POD,g − V_FE‖_2 / ‖V_FE‖_2, g = 1, ..., G
    k ← min(ε)
    j ← j + 1
  until j ≤ r
end
```

III. Driven Cavity Example

We apply the methodologies developed in the previous section to the flow in a controlled driven cavity. Driven cavity flows are a canonical problem in fluid mechanics [15,16] and are of great importance because of their application to industrial processes and their use as a benchmark for two-dimensional incompressible Navier–Stokes solvers. Therefore, this geometry has been the subject of much study in flow control problems.

A. Geometry and Test Conditions

Figure 2 illustrates the geometry of the square cavity considered in this work. It is a two-sided lid-driven cavity in which the upper and lower walls Γ_T and Γ_B move independently of each other. Each wall translates periodically at an identical speed and frequency, but the oscillation of the lower wall lags that of the upper wall by a phase lag

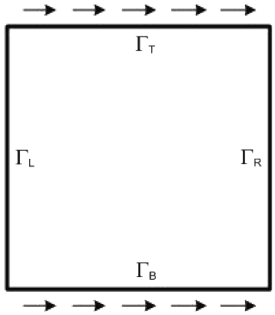

Fig. 2 Schematic of a driven square cavity.

ϕ. This phase differential influences the flow physics inside the cavity and functions as an actuator. The side dimension of the cavity is 1.0 cm.

The boundary conditions of the cavity are represented as

$$\begin{Bmatrix} u \\ v \end{Bmatrix} = \begin{Bmatrix} 0 \\ 0 \end{Bmatrix} \quad \text{on } \Gamma_L, \Gamma_R \qquad \begin{Bmatrix} u \\ v \end{Bmatrix} = \begin{Bmatrix} U_0 h_0(t) \\ 0 \end{Bmatrix} \quad \text{on } \Gamma_T$$
$$\begin{Bmatrix} u \\ v \end{Bmatrix} = \begin{Bmatrix} U_0 \beta(t) \\ 0 \end{Bmatrix} \quad \text{on } \Gamma_B \tag{32}$$

The functions $h_0(t)$ and $\beta(t)$ are defined as

$$h_0(t) = \sin(2\pi f t) \qquad \beta(t) = \sin(2\pi f t - \phi) \tag{33}$$

For the driven cavity, the parametric space is defined as $\Lambda = (Re, \phi)$.

Table 1 Test matrix values for driven cavity

Parameter	Value
U_0, cm/s	1.0
f, Hz	1.0
Re	[100 200 300 400 500 600 700 800 900 1000]
ϕ, deg	[150 160 170 180 190 200 210]

By adjusting the kinematic viscosity of the fluid and the phase lag between walls, it is possible to simulate the cavity flow for various points in the parametric space. A test matrix for the driven cavity is displayed in Table 1. The transient solution is computed from the initial condition, which is the steady-state solution of the driven cavity flow with boundary conditions $\{u, v\} = 1$ at the top wall and $\{u, v\} = 0$ elsewhere. The flow is simulated for 10 cycles and data are collected at 100 intervals during the final cycle. For each (Re, ϕ) combination, reduced-order models are generated using the POD procedures described in Sec. II.

B. Simulation Results

1. Flow Physics

A collection of flowfields is obtained by varying the parameters in Λ. The simulations in this case are open-loop and are performed using the full-order models. All time and velocity data in the plots are nondimensionalized. A finite element formulation with a uniformly spaced structured grid composed of 45×45 nodes and bilinear quadrilateral basis elements is used to simulate the flow physics. Additionally, the simulation results are compared with that obtained

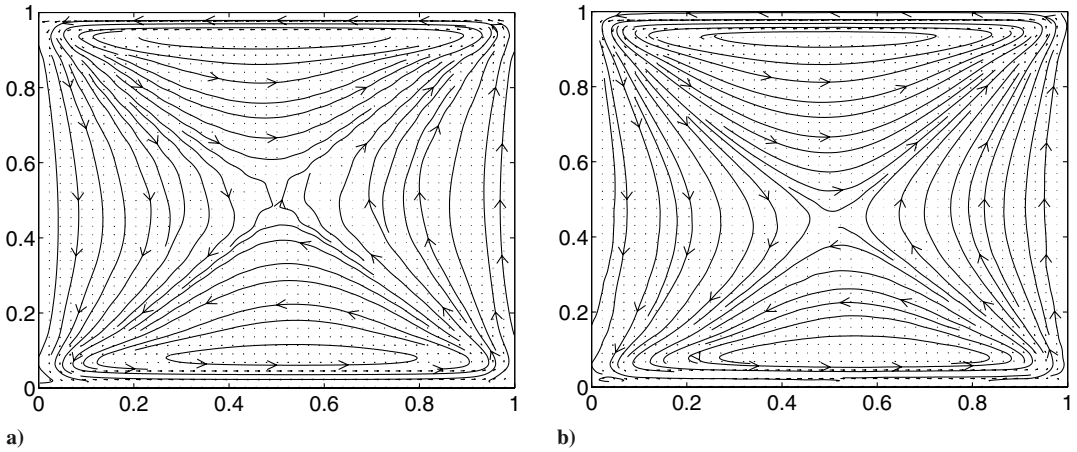

Fig. 3 Velocity field at $t = 10$ and $(Re, \phi) = (100, 150 \text{ deg})$: a) structured grid and bilinear basis elements and b) unstructured grid and Lagrange-quadratic basis elements.

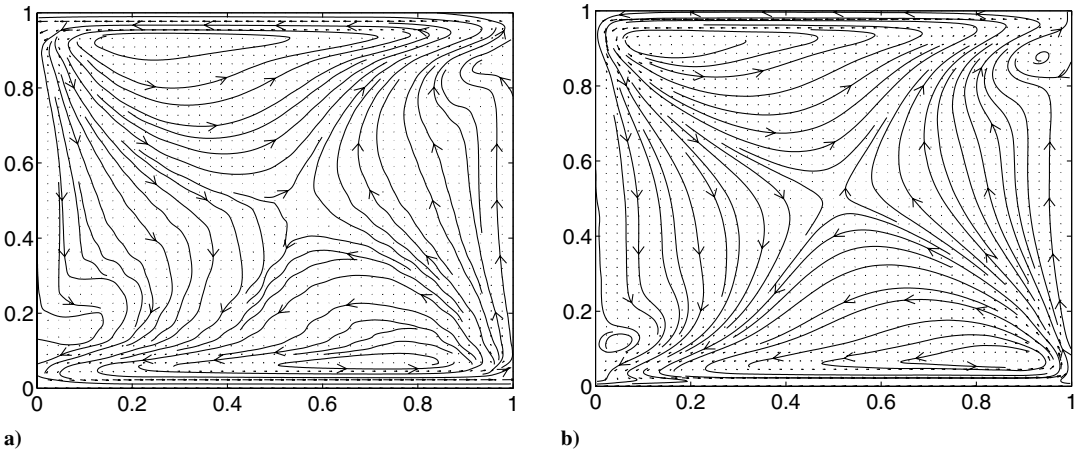

Fig. 4 Velocity field at $t = 10$: $(Re, \phi) = (1000, 210 \text{ deg})$: a) structured grid and bilinear basis elements and b) unstructured grid and Lagrange-quadratic basis elements.

using COMSOL Multiphysics. In this case, the grid is unstructured with 1740 triangular Lagrange-quadratic basis elements.

Figures 3 and 4 show two typical flowfields corresponding to the points $(Re, \phi) = (100, 150 \text{ deg})$ and $(Re, \phi) = (1000, 210 \text{ deg})$ in the test matrix. A snapshot of the velocity fields is taken at $t = 10$ s, which is at the end of the simulation period. The flow shape typically consists of two large vortices circling at the top and bottom halves of the cavity, with opposite rotations. Additionally, in Fig. 4, a small recirculation region appears alongside each large vortex. A qualitative comparison of the transient flowfields, each corresponding to a different point in Λ, was carried out to demonstrate the influence of the chosen parameters. A similar comparison is shown in Fitzpatrick et al. [5] for Stokes flow. For both elements in the parametric set, the flowfields are similar in both finite element implementations, which indicates that the simulation results are grid-independent.

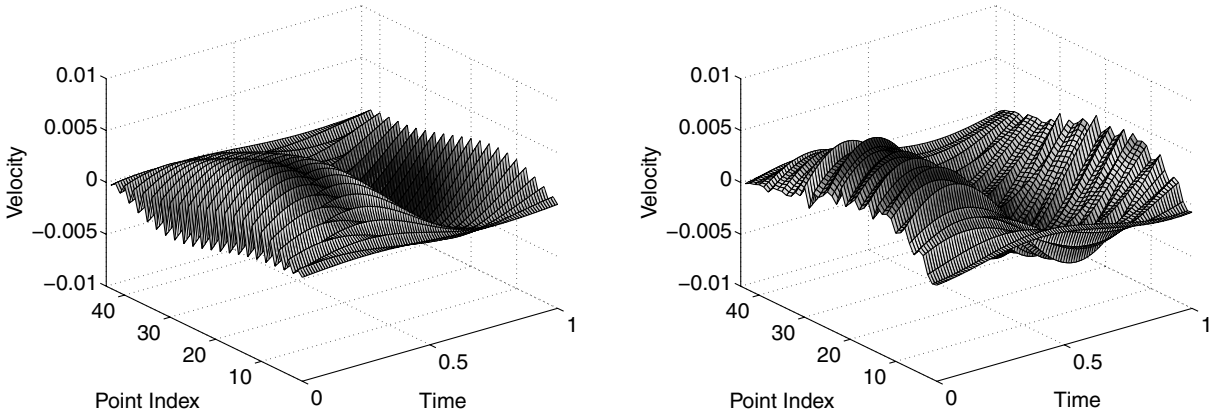

Fig. 5 Velocity field at $t = 10$: $(Re, \phi) = (100, 150 \text{ deg})$: a) structured grid and bilinear basis elements and b) unstructured grid and Lagrange-quadratic basis elements.

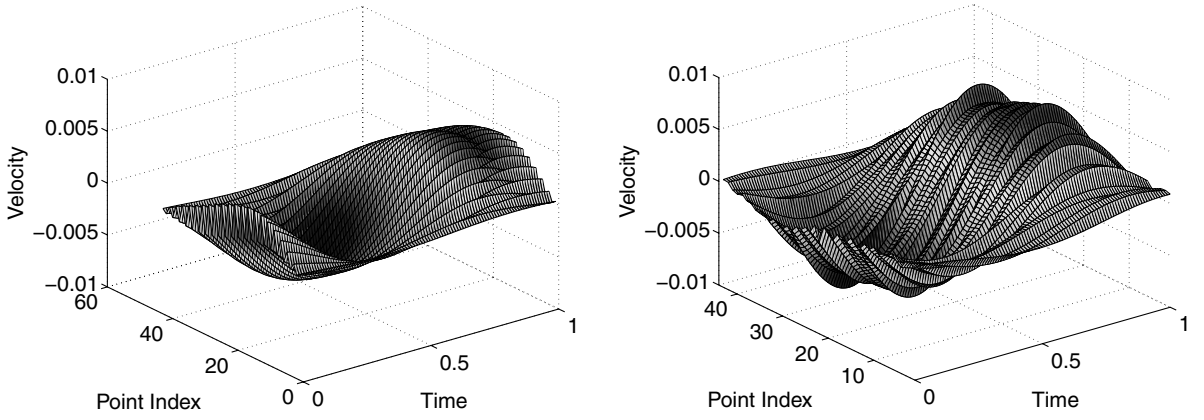

Fig. 6 Velocity field at $t = 10$: $(Re, \phi) = (100, 210 \text{ deg})$: a) structured grid and bilinear basis elements and b) unstructured grid and Lagrange-quadratic basis elements.

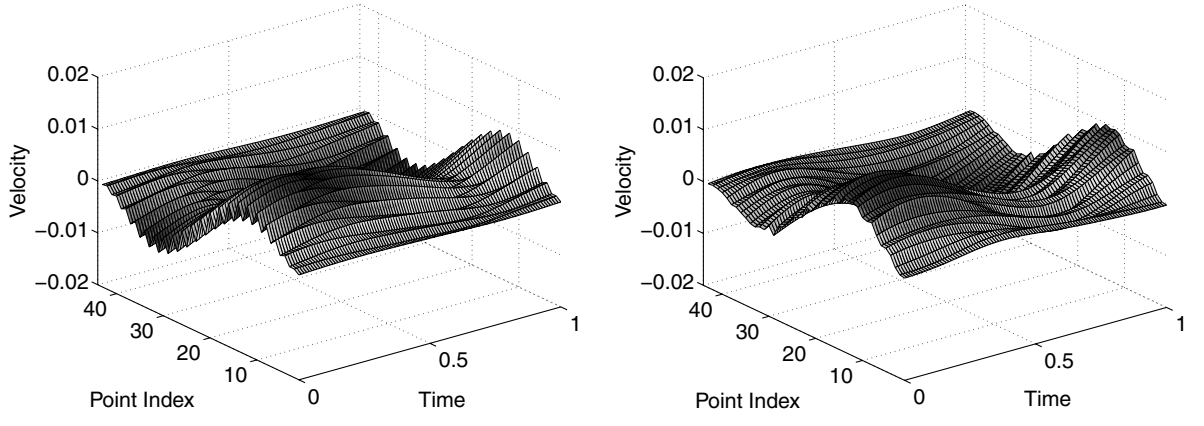

Fig. 7 Velocity field at $t = 10$: $(Re, \phi) = (1000, 150 \text{ deg})$: a) structured grid and bilinear basis elements and b) unstructured grid and Lagrange-quadratic basis elements.

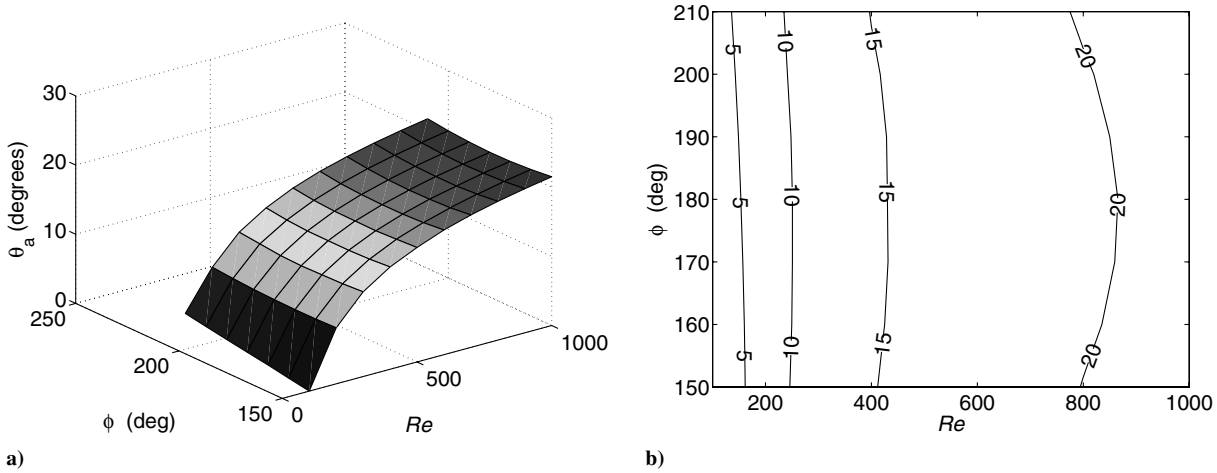

Fig. 8 Voxel relative to $(Re, \phi) = (100, 150$ deg): a) surface plot and b) contours.

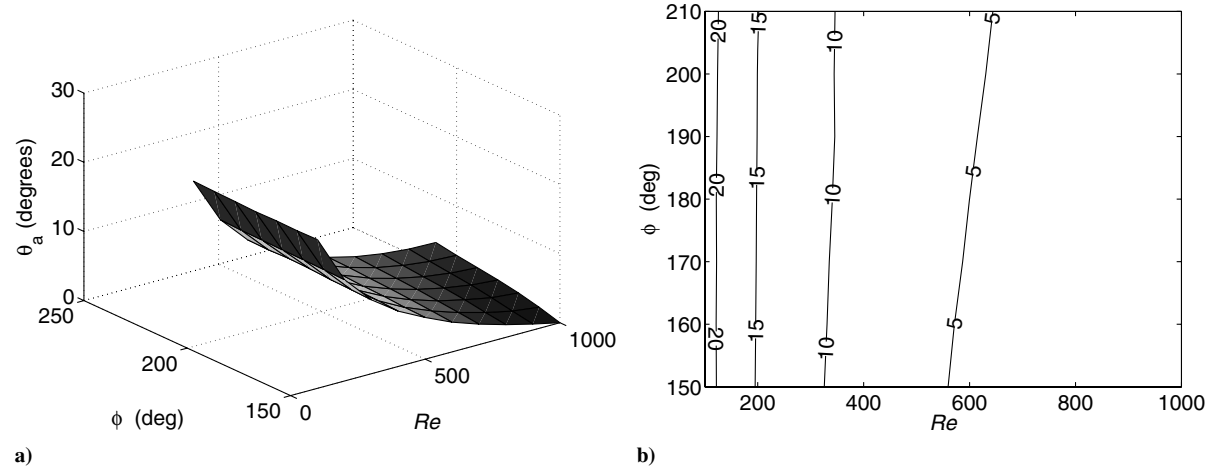

Fig. 9 Voxel relative to $(Re, \phi) = (1000, 150$ deg): a) surface plot and b) contours.

Figures 5–7 present three-dimensional plots of this horizontal velocity as a function of time. The data for the plots are generated from 19 sensors that are located on the horizontal midsection of the cavity. Figure 5 shows the velocity plot of the full-order open-loop flow when $(Re, \phi) = (100, 150$ deg). The plot shows a sinusoidal variation of the velocity at the top and bottom boundaries. The magnitude overall is very small, showing the low horizontal movement in this cross section of the cavity. The maximum value is 0 and the minimum is -0.04, which occurs at $t = 0.65$ and sensor point 12. A similar plot for the case $(Re, \phi) = (100, 210$ deg) is shown in Fig. 6. Again, a sinusoidal variation is observed and the overall shape resembles that of the previous figure. The maximum is zero and the minimum is -0.052, which occurs at $t = 0.63$ and sensor point 12. Figure 7 shows the velocity plot for $(Re, \phi) = (1000, 150$ deg). The magnitude of the velocity is in the same range as the previous two plots, but the overall shape is very different. The maximum velocity is 0.02, which occurs at $t = 0.15$ and sensor point 5; the minimum is -0.01 at $t = 0.65$ and sensor point 17. Compared with the velocity for $(Re, \phi) = (100, 150$ deg) and $(Re, \phi) = (100, 210$ deg), the magnitude and phase are different.

2. *Subspace Angle Metric*

We present surface and contour plots of the subspace angle metric to evaluate its variation over the parametric space. Figure 8 shows the distribution of the metric relative to the "voxel" at $(Re, \phi) = (100, 150$ deg). The value of the metric ranges from 0 deg, where the parametric case in question is being compared with itself, to a maximum value of around 22 deg at $(Re, \phi) = (1000, 210$ deg). Figure 8b illustrates a stronger dependence of the subspace angle metric on the Reynolds number than on the phase differential.

Figure 9 displays the subspace angle metric relative to the parametric case $(Re, \phi) = (1000, 150$ deg). Here, the distribution is different from that observed in Fig. 8, in that the subspace angle increases more slowly as we move away from the reference point and then more rapidly near the opposite end of the test matrix. As in Fig. 8, the variation between velocity fields for different points in the parametric space are more dependent on the Reynolds number than

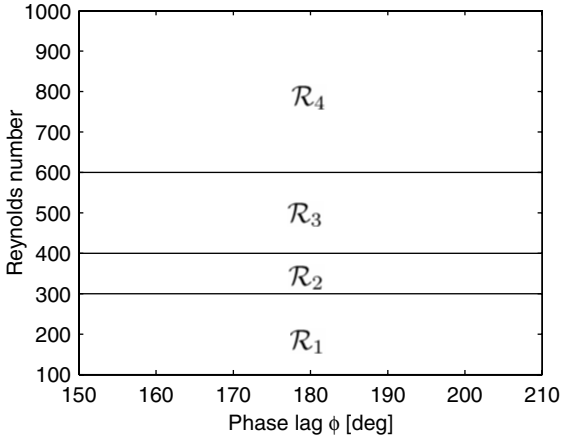

Fig. 10 Partition of parametric space (Re, ϕ).

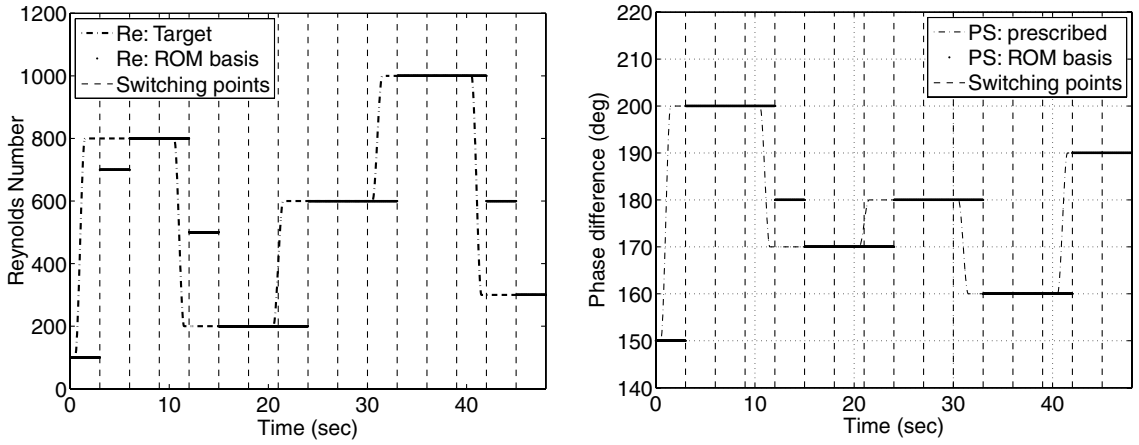

a) Reynolds number **b) Phase differential**

Fig. 11 Open-loop results for switched model of driven cavity; switching intervals are at 3 s.

on the phase differential, but some sensitivity to phase differential can be observed at higher Reynolds numbers.

3. Partition of Parametric Space

Figure 10 displays the parameter space partitioned into regions using the procedures in Sec. II.C. A threshold value of $a_{\text{th}} = 0.95$ is used to generate the regions. The following subspaces are determined for the driven cavity:

$$\mathcal{R}_1 = \{(Re, \phi) | Re \in [100, 300)\}$$

$$\mathcal{R}_2 = \{(Re, \phi) | Re \in [300, 400)\}$$

$$\mathcal{R}_3 = \{(Re, \phi) | Re \in [400, 600)\}$$

$$\mathcal{R}_4 = \{(Re, \phi) | Re \in [600, 1000)\}$$

The parametric space is partitioned into slabs of varying thickness, which indicates that the "distance" of the spanning subspace of a given velocity field from the chosen reduced-order basis in a given region is much more dependent on the Reynolds number than on the phase lag. This kind of partition makes sense based on observations of the flow physics and the distribution of the subspace angle metric as a function of the flow and actuation parameters. Even though the phase differential has a greater effect on the flowfield at higher Reynolds numbers, the subspace angle distribution exhibits a smaller gradient for that part of the regime, which is reflected in the thicker slab of the region $\mathcal{R}_4$.

4. Open-Loop Simulation

To create the switched dynamic system, a reduced-order basis is selected for each region $\mathcal{R}_i$ and a switching law developed using the procedures in Sec. II.D. An open-loop simulation of the full-order finite element model is executed when the Reynolds number and phase differential are varied smoothly through the operating domain. The switched dynamic system is simulated for identical initial conditions, with switching instants every 3 s. Figure 11 compares the trajectories of the Reynolds number and phase differential from the open-loop simulations of the two models. The switched reduced-order model is able to satisfactorily match the trajectories of the flow and actuation parameters, but there are discrepancies between the trajectories of both models when the parameters vary across switching intervals. It is expected that the length of the switching interval has a strong influence on the ability of the switched model to track the parametric trajectory of its full-order counterpart.

IV. Conclusions

A new approach is proposed to evaluate the use of multiple reduced-order models in the form of a wandering-subspace problem. These models use a formulation based on the POD decomposition. A subspace angle metric is defined and used to group similar regions in the domain of flowfields over the range of parameters. It is shown that the angle between subspaces is an effective measure of the similarity between velocity fields for different points in the parametric space. This knowledge can be used to develop partitions of the parametric space, from which a switched dynamic system can be derived.

The methodology is applied to the modeling of a two-dimensional two-sided driven cavity, and open-loop simulations demonstrate the ability of the switched reduced-order model to approximate the parametric trajectories of the full-order model. Experience with the switched model indicates that it will be necessary to address the minimum switching interval for maximum desired accuracy of the model, the selection of the reduced-order bases in each region, and the number of reduced-order modes required for satisfactory control performance.

Future work will refine the modeling approach through a more systematic selection of representative reduced-order bases in a region and the application of estimation algorithms for hybrid systems. Another goal is to derive and implement controllers for the switched dynamic system using either gain-scheduling, linear parameter-varying, or switching approaches.

Acknowledgment

The primary author was supported by a National Research Council Research Associateship at the U.S. Air Force Research Laboratory, Munitions Directorate.

References

[1] Lofdahl, L., and Gad-el Hak, M., "MEMS Applications in Turbulence and Flow Control," *Progress in Aerospace Sciences*, Vol. 35, No. 2, 1999, pp. 101–203. doi:10.1016/S0376-0421(98)00012-8

[2] Huang, A., Lew, J., Xu, Y., Tai, Y.-C., and Ho, C.-M., "Microsensors and Actuators for Microfluidic Control," *IEEE Sensors Journal*, Vol. 4, No. 4, 2004, pp. 494–502. doi:10.1109/JSEN.2004.830949

[3] Bewley, T., Temam, R., and Ziane, M., "A General Framework for Robust Control in Fluid Mechanics," *Physica D*, Vol. 138, Nos. 3–4, 2000, pp. 360–392. doi:10.1016/S0167-2789(99)00206-7

[4] Burns, J. A., King, B. B., and Rubio, D., "On the Design of Feedback Controllers for a Convecting Fluid Flow via Reduced Order Modeling," *IEEE International Conference on Control Applications*, Vol. 2, Inst. of Electrical and Electronics Engineers, Piscataway, NJ, 1999, pp. 1157–1162.

[5] Fitzpatrick, K., Feng, Y., Lind, R., Kurdila, A. J., and Mikolatis, D. W., "Flow Control in a Driven Cavity Incorporating Excitation Phase Differential," *Journal of Guidance, Control, and Dynamics*, Vol. 28, No. 1, 2005, pp. 63–70.

[6] Ravindran, S. S., "Reduced-Order Adaptive Controllers for Fluid Flows Using POD," *Journal of Scientific Computing*, Vol. 15, No. 4, 2000,

pp. 457–478.
doi:10.1023/A:1011184714898

[7] Fahl, M., "Trust-Region Methods for Flow Control Based on Reduced Order Modeling," Ph.D. Thesis, Univ. Trier, Trier, Germany, Dec. 2000.

[8] Jørgensen, B. H., Sørensen, J. N., and Brøns, M., "Low-Dimensional Modeling of a Driven Cavity Flow with Two Free Parameters," *Theoretical and Computational Fluid Dynamics*, Vol. 16, No. 4, 2003, pp. 299–317.
doi:10.1007/s00162-002-0082-9

[9] Branicky, M. S., Borkar, V. S., and Mitter, S. K., "A Unified Framework for Hybrid Control," *33rd IEEE Conference on Decision and Control*, Vol. 43, No. 1, Inst. of Electrical and Electronics Engineers, Piscataway, NJ, 1994, pp. 31–45.

[10] Liberzon, D., *Switching in Systems and Control*, Birkhauser, Boston, 2003.

[11] Rediniotis, O. K., Ko, J., and Kurdila, A. J., "Reduced Order Nonlinear Navier–Stokes Models for Synthetic Jets," *Journal of Fluids Engineering*, Vol. 124, No. 2, 2002, pp. 433–443.
doi:10.1115/1.1467598

[12] Seidman, T. I., "Optimal Control for Switching Systems," *Proceedings of the 21st Conference on Information Sciences and Systems*, Johns Hopkins Univ., Baltimore, MD, 1987, pp. 485–489.

[13] Golub, G. F., and van Loan, C. F., *Matrix Computations*, 3rd ed., Johns Hopkins Univ. Press, Baltimore, MD, 1996.

[14] Dodel, S., Herrmann, J. M., and Geisel, T., "Functional Connectivity by Cross-Correlation Clustering," *Neurocomputing: Variable Star Bulletin*, Vols. 44–46, June 2002, pp. 1065–1070.
doi:10.1016/S0925-2312(02)00416-2

[15] Shankar, P. N., and Deshpande, M. D., "Fluid Mechanics in the Driven Cavity," *Annual Review of Fluid Mechanics*, Vol. 32, 2000, pp. 93–136.
doi:10.1146/annurev.fluid.32.1.93

[16] Blohm, C., and Kuhlman, H. C., "The Two-Sided Lid-Driven Cavity: Experiments on Stationary and Time-Dependent Flows," *Journal of Fluid Mechanics*, Vol. 450, 2002, pp. 67–95.
doi:10.1017/S0022112001006267

C. Kaplan
Associate Editor